06

Laser evaporation of cerium-yttrium complex oxide targets for plasma component separation applications

© N.N. Antonov, S.D. Kuzmichev, M.D. Platonov, A.O. Serov

Joint Institute for High Temperatures, Russian Academy of Sciences,
Moscow, Russia
e-mail: platonov.md@yahoo.com

Received September 11, 2025
Revised November 1, 2025
Accepted November 13, 2025

The concept of plasma separation of oxide mixtures includes, as one of its stages, the conversion of these mixtures into a plasma flow. In the framework of this work, an experimental study was conducted on the processes of converting a condensed mixture of model substances into the vapor phase using radiation from a quasi-continuous laser with a wavelength of 1067 nm. The possibility of evaporating in vacuum a target consisting of a mixture of refractory complex oxides of cerium and yttrium has been experimentally demonstrated. The evaporating productivity was about 10 grams per hour in conditions required for a vapor source in the plasma component separation process. The radiation power density, at which an optimal relationship between the rates of evaporation and undesirable production of coarse-dispersed particles in the target disintegration products is observed, has been determined, namely at a level of $1 \cdot 10^6$ W/cm^2. At the non-stationary stage of the process, incongruent evaporation of components is observed, which can subsequently be used for enriching the target material with the least volatile components. The implementation of such enrichment will conceptually allow reducing the requirements for the productivity of the plasma separation process.

Keywords: laser evaporation, plasma separation, rare-earth oxides, fiber lasers.

DOI: 10.61011/TP.2026.03.63166.260-25

Introduction

For implementing plasma separation of spent nuclear fuel (SNF) by component mass groups, a technique for evaporation of initial substances, their ionization mechanisms and procedure for plasma flow supply to a separation chamber shall be developed [1]. This work addresses laser evaporation as one of possible techniques for producing refractory oxides vapor for this process. Requirements for plasma separation vapor source imply that a substance evaporation rate reaches hundreds of grams per hour with the minimum amount of debris, drops and clusters in the vapor flow. Most of current studies of laser evaporation processes are focused on dense uniform film deposition via vapor condensation on a substrate (pulse laser deposition, PLD). Achievement of plasma or single-phase vapor flow is a key prerequisite for successful fulfillment of these processes. The use of ultrashort low-energy radiation pulses serves here as the key focus area. However, efficiency in this case turns out to be insufficient for solution of plasma separation problems, and specific energy consumption turns out to be inacceptable. Thus, for example, forced reduction of the pulse energy below $1\,\mu$J with a picosecond duration and power density of $I_0 \sim 10^{11}-10^{12}$ W/cm^2 leads to a significant reduction of gas phase condensation probability. However, the highest measured mean drop-free metal ablation rate reaches only 1 g/h with the highest possible mean radiation power of the used lasers [2,3]. The use of ultrashort pulses for the purpose of separation is also limited by the fact that highly ionized plasma with an ion energy of 100 eV and higher occurs at $I_0 \geq 10^{10}$ W/cm^2, preventing from effective separation of elements in crossed electric and magnetic fields in the separation chamber. A higher evaporation rate is achieved when using quasi-continuous lasers with a pulse duration of hundreds of microseconds. Efficiency of oxide nanoparticle production (Y_n) via laser evaporation in buffer gas, in particular, air, can serve as a reference for estimating the mean evaporation rate (Y). This is proved by conclusion made in [4], where it is shown that at a power density on the order of 10^6 W/cm^2, which is typical of this case, vapor condensation Y_n occurs only when vapor is mixed with air. Maximum values of Y_n depend on thermodynamic properties of evaporated oxides and radiation variables. For example, Y_n 90 g/h was achieved via zirconium oxide evaporation by CO_2-laser with a mean power of 4 kW with a spot power density at 10^6 W/cm^2 [5], via evaporation of the CeO_2 and Gd_2O_3 mixture by CO_2-laser with a mean power of 665 W$-$60 g/h [4]. Near-infrared (IR) optical fiber lasers with lower mean power provide a little lower efficiency [6], however, it shall be considered that energy efficiency of optical fiber lasers in these processes is several-fold higher than that of CO_2-lasers. Weak radiation absorption in the material is one of the known causes of insufficient efficiency and substance flashing under the target surface with discharge of overlying fragments. For example, this is the case when using near-IR radiation for oxide evaporation in air [6]. However, it is known that at high temperatures in some oxides, near-

IR radiation absorption coefficient increases with heating, and doesn't decrease after cooling down in case of vacuum fusion. The effect in pure substance is explained by the increase in oxygen vacancy concentration in the main crystal lattice, but there is no explicit explanation for the case when a material contains impurities [7]. The foregoing justify the conclusion concerning the validity of experimental study of using high-efficiency and user-friendly near-IR optical fiber lasers for oxide mixture vacuum evaporation in conditions corresponding to the vapor source requirements for plasma separation of components.

Nonradioactive rare-earth metal oxides can serve as model substances for conducting experiments for the development of SNF plasma separation technique [8]. Moreover, stoichiometric cerium dioxide up to the temperature of 1673 K is close to uranium dioxide by its thermal-physical properties [9].

The objective of this work was to study pulsed laser evaporation (using 1067 nm optical fiber laser) of targets made of the Y_2O_3 and CeO_2 mixture, which simulate SNF components during conversion of the condensed substance into a plasma flow. The main analyzed variables are: condensed mixture evaporation rate, amount of coarse fraction, vapor and target composition behavior at different evaporation stages.

1. Experimental procedure and conditions

This work describes the results of study of laser evaporation of cerium and yttrium oxide mixture targets (hereinafter referred to as CeO_2+Y_2O_3 targets) with the atomic ratio [Y]:[Ce] = 1:1.14, and ceramic targets containing only simple oxides of these elements. Diameter of cylindrical targets is 18 mm, height is 15 mm. The amount of impurities in the target is max. 20 ppm (according to the manufacturer RPF Luminophor). According to the X-ray diffraction analysis (XPA), the initial oxide mixture target contains three crystal phases: complex oxides $Y_{0.6}Ce_{0.4}O_{1.7}$, $Y_{0.3}Ce_{0.7}O_{1.85}$ and yttrium oxide Y_2O_3.

Target evaporation used 1067 nm quasi-continuous fiber laser (with output power modulation) (IPG Photonics) with a M_2 laser beam parameter of 1.05. Laser is interfaced with a collimation, beam focusing and target scanning system via programmed algorithms (ATEKO NM). The beam was Gaussian, diameter of the focused light beam at the target by the power density reduction level up to 13.6 % was 0.13 mm. Raster scanning of the upper base of the cylindrical target was set, the number of surface passes was from 1 to 8 (each pass included scanning by two perpendicular rasters). The maximum scanning time as 2 min. Raster line density was set to 20 mm^{-1}. The beam during a shot moved with respect to the target, evaporation region density on each line was also set to 20 mm^{-1}. According to the set mode, radiation spots from consecutive shots partially overlapped on the lines. Beam travel speed between shots (including movement between lines) was 5 m/s. Laser pulse duration was set to 100 μs (pulse and no-load durations on the raster line are the same for this type of modulation).

For estimating the developed evaporation thresholds of CeO_2 and Y_2O_3, the following was assumed. Since the radiation spots partially overlapped during scanning, radiation hit the preheated target surface; this was displayed as bright afterglow of the scanned surface. Therefore the developed evaporation thresholds of CeO_2 and Y_2O_3 were estimated using the most high-temperature values of thermal-physical variables of solid stoichiometric oxides [9–11]. With our experiment setup, the following condition is met

$$t_{imp} \ll r_{las}^2/\chi$$

where r_{las} is the light spot radius, χ is the thermal diffusivity, t_{imp} is the laser pulse duration.

This means that heat-conduction loss of energy in transverse direction can be ignored.

Time threshold of steady-state („developed") evaporation during the laser pulse (t_{evp}) for simple oxides was estimated using the following equation [12,13]:

$$t_{evp} = \frac{L_{evp}^2 \rho^2 \chi}{(1-R)^2 I_0^2},$$

where L_{evp} is the specific heat of evaporation, ρ is the bulk density, R is the reflection coefficient, I_0 is the incident radiation power density. The threshold is overcome ($t_{evp} \ll 100\,\mu$s): for CeO_2 — almost throughout the used intensity range; for evaporation of Y_2O_3 — only at intensities higher than $2 \cdot 10^6$ W/cm^2, which are close to the maximum values for the laser and focusing system used for operation.

Placement of the target in the chamber with a volume of about 1 m^3 was determined by the need to take into account the plasma separation system requirement, where the ion trajectory radius is equal to several tens of centimeters [1]. This requirement defined the placement of the target at a significant distance (80 cm) from the optical input window at $\sim 45^\circ$ to the evaporated surface; target surface was arranged horizontally. Such arrangement significantly reduced contamination of the coated input window by evaporation products, nevertheless, to ensure its protection, additional replacement optical glasses with coating at 1067 nm were placed in the chamber, and their transmittance was checked periodically by measuring the mean radiation power transmitted through the glasses to the chamber (using theUP55-600F-HD Gentec EO). Residual air pressure in the chamber was set to 0.04 Pa. Mean radiation power in the target region during the experiments was as high as 250 W, I_0 — $2.3 \cdot 10^6$ W/cm^2 with the maximum laser pulse power. Collector for trapping the evaporated substance is a knockdown hollow metal cylinder with a diameter of 100 mm, that totally encompasses the target and has openings for light input and attachment of small polished silicon substrates (10×20 mm). Photograph

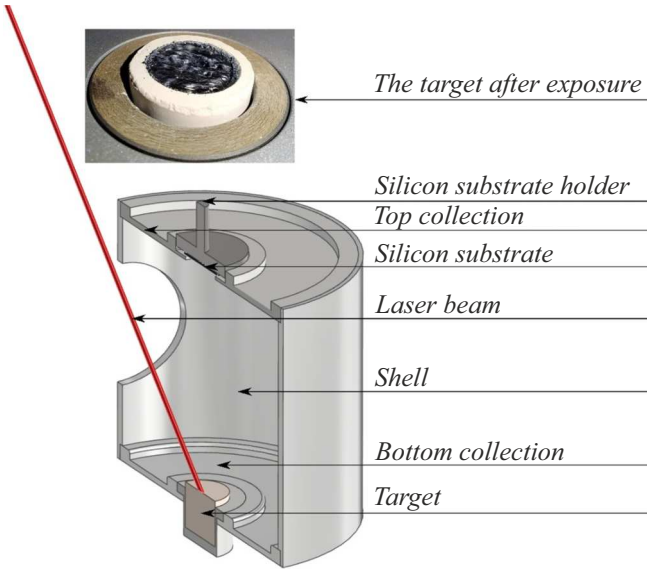

Figure 1. Experimental module and CeO_2+Y_2O_3 target after exposure to $1.5 \cdot 10^6$ W/cm^2 laser and one pass.

of the experimental module and targets after laser exposure is shown in Figure 1.

Mean target destruction speed and destruction product collection efficiency of the collector were measured by comparing the corresponding weights measured before and after evaporation. Formation of film coating was detected only on the shell and on top of the collector assembly. At the same time, products of destruction (drops and debris) larger than 15 μm were not held on the shell and on top of the collector and were accumulated on the lower collector (except for those that left the region of interest through a side opening in the collector designed for laser radiation input). Drops and debris mainly with micron and submicron sizes were built into the film on the top and sides of the collector. Their weight was estimated from the analysis of SEM images and was max. 2% from the film weight.

Vapor composition in the chamber during target evaporation was measured using the RGA300XTM quadrupole mass analyzer. Images of films deposited on the collector via vapor condensation and of target surfaces, and their elemental composition were obtained using the LEO 1430 SEM with the INCA system for energy-dispersive X-ray analysis (EDX). Diffuse reflectance spectra of targets before and after evaporation were measured using the SF-56 spectrophotometer with a diffuse reflectance system. To identify the phase composition of initial targets and solidified melt formed on the surface, diffraction patterns were made using the Rotaflex RU-200 X-ray source with a rotating copper anode (Rigaku, Japan), ICDD PDF-2 powder diffraction database was used for phase search [14].

Thermogravimetric analysis (TGA) with differential scanning calorimetry of the solidified melt was carried out using the TA Instruments SDT Q600 analyzer.

2. Results and discussion

2.1. Evaporation rate and change in the target surface properties during radiation exposure

A series of experiments was carried out at the initial research phase to obtain evaporation rate Y data depending on the laser power density I_0 for three types of targets: CeO_2, Y_2O_3, CeO_2+Y_2O_3. The measurement results are shown in Figure 2.

Relative measurement error of oxide mass evaporation rates (three measurements for each point) was max. 4% in the range of I_0 lower than $1.5 \cdot 10^6$ W/cm^2 and 7% for higher values of I_0.

The maximum measured value of Y is close to Y_n during oxide ceramics evaporation by pulsed CO_2-laser as obtained in [4,5]. Note that the mean radiation power in our case (up to 250 W) is lower, and optical fiber laser absorption properties of the initial materials of interest are worse than those of CO_2-laser. The difference of our experiment is in that evaporation is performed without oxygen, due to which optical properties of the initial surface vary significantly. The surface of the opaque melt of CeO_2 and CeO_2+Y_2O_3 targets formed in vacuum is dark gray, and the surface of the Y_2O_3target melt is black, and this color doesn't changes later when a target is stored in air.

Diffuse reflectance spectra of the initial target surface and solidified melt prove the provided visual observation and are shown in Figure 3.

The observed change in the optical properties of the target can lead to considerable fluctuations of the vaporous fluid production rate in the plasma converter and also considerably affect the composition of the generated plasma. Investigation of the target materials consisting of pure simple oxides, CeO_2 and Y_2O_3, didn't detect any apparent differences between the composition and structure of the initial samples and solidified melt samples due to insufficient

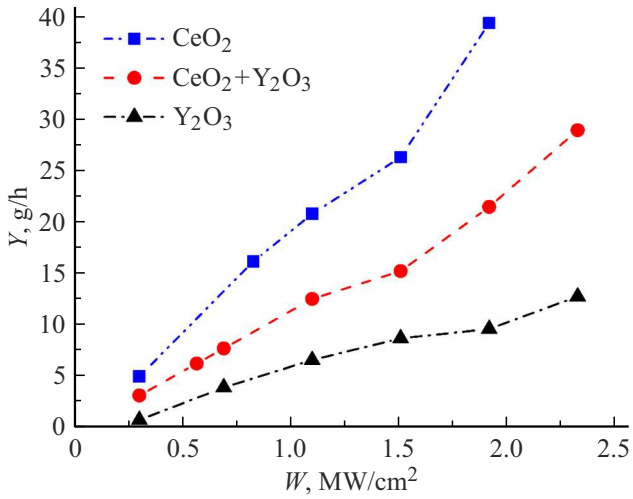

Figure 2. Oxide mass evaporation rates vs. radiation power density in a 0.13 mm spot.

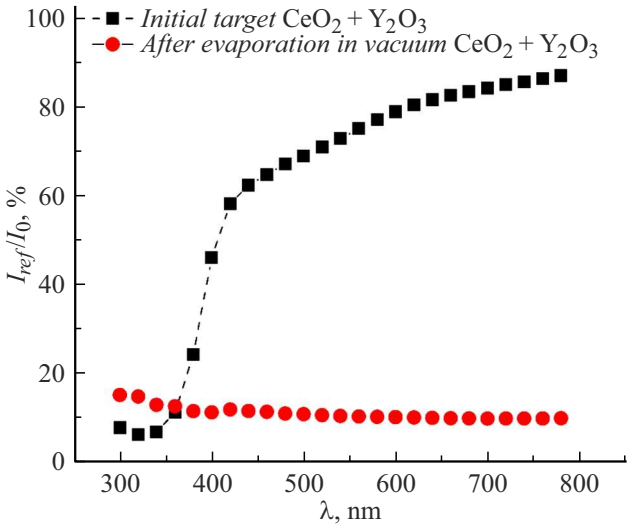

Figure 3. Diffuse reflectance spectra of targets.

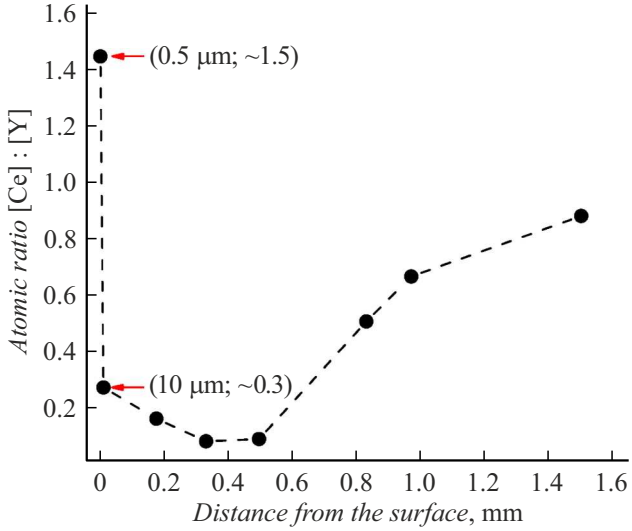

Figure 4. [Ce]:[Y] distribution over the target depth after the first pass.

sensitivity of the employed techniques. However, for plasma separation purposes, investigations of evaporation processes and properties of complex mixed oxides are of the paramount interest, and in this case changes were detected in the CeO_2+Y_2O_3 target material during evaporation in vacuum. It was found that cerium-/yttrium-containing crystal phases in the solidified CeO_2+Y_2O_3 target melt had changed, i.e. $Y_{0.73}Ce_{0.27}O_{1.635}$ and $Y_{0.497}Ce_{0.503}O_{1.751}$ phases had appeared.

During TGA, when the solidified complex oxide melt was heated in air, its weight increased by more than 1 % as the temperature increased to 550 °C. Heat was released simultaneously. Upon completion of TGA, the sample returned to the original off-white color of the initial target. These results suggest that melt heating in air leads to oxidation. This means that exposure of the CeO_2+Y_2O_3 mixture target to laser radiation led not only to a change in the target material composition, but also to violation of stoichiometry of its components resulting in oxygen deficiency. Note that the $Y_{0.497}Ce_{0.503}O_{1.751}$ melt phase is characterized by a higher oxygen mobility at low temperature due to the presence of large amount of oxygen vacancies [15]. In our case, additional defects during evaporation in vacuum led to an increase in radiation absorption in the melt compared with the initial target (Figure 3). This increase shall affect the relation between the rate of lase evaporation from melt and the rate of evaporation from the initial oxide ceramics. Investigation of the scale of this effect will be the topic of future work.

Figure 4 shows the [Ce]:[Y] distribution over the target depth after one pass with power density $1.1 \cdot 10^6$ W/cm^2.

A point near zero was obtained by the EDX analysis of the top melt surface with the probing electron beam striking the surface from above, therefore the point characterizes a mean value of [Ce]:[Y] over the depth from zero to a depth of about 0.5 μm, with the largest contribution of elements located on the surface; other given values were obtained by analyzing the material at the fracture of the evaporating target. In points measured via the fracture analysis, the expected cerium depletion attributed to prevailing evaporation of CeO_2 is observed. After achievement of the minimum at a depth of 0.3–0.4 mm within the melt, cerium concentration gradually grows with depth and is almost restored to the initial level at 1 mm from the surface. At the same time, when the melt is analyzed on the surface, rather than on the fracture side, high relative concentration of cerium is detected on the surface. This can result from redeposition on the surface of a part of cerium oxide abundantly evaporated during the first pass. This is facilitated by occurrence of a complex relief on the target surface after the first laser shots. A cerium-enriched thin surface layer formed on the protruding relief elements partially shields the underlying melt, therefore it gives a large contribution to the cerium concentration measured by the EDX technique, despite a small thickness of this layer.

2.2. Vapor phase and deposited film

For plasma separation of SNF, the presence of significant concentration of complex decay element oxide molecules or clusters in the separated plasma flow, which is typical of cluster evaporation of many substances by laser radiation in our power density range, is inadmissible [16]. According to the developed separation procedure, a plasma flow is formed from the vapor flow using a special discharge before input into the separator. Initial composition of the working medium flow is an important variable in this process because the possible presence of complex oxide molecules in vapor will lead to a need for increasing the discharge energy to provide molecule dissociation.

The study investigated vapor composition using a quadrupole mass-spectrometer placed at a distance of 100 cm from the target at 45° to the evaporation surface. Since evaporation is not a steady-state and uniform process, a spectrum form obtained by averaging several tens of mass spectra is represented as the measurement results. Among ions, the presence of which is important for processing plasma separation, Ce^+, CeO^+, CeO_2^+ and YO^+ are observed (Figure 5) during laser evaporation of two-component ceramics in the mass-spectrometer. The composition of cerium-containing ions qualitatively corresponds to the composition observed during evaporation from effusion tantalum cell at 2600 K in [17]. In the measurement conditions [17], the presence of Ce^+ in the spectrum is explained by monoxide fragmentation within the spectrometer's ion source. The difference of our evaporation conditions and high peak ratio of CeO^+ and Ce^+ do not allow to state that the presence of Ce^+ is exclusively an instrument function of the mass-spectrometer. The obtained spectrum has no Y^+, which is observed during evaporation of Y_2O_3 from the effusion cell [18]. Moreover, the presence of Y^+ in [18] indicates that there are atoms of this metal specifically in vapor, in an amount of about 1 %.

During evaporation of CeO_2+Y_2O_3 mixtures, not only stable molecules, but also radicals are observed, therefore the next plasma separation phase shall include the analysis of oxide evaporation product distribution by weights, consideration of differences in ionization efficiency and in lifetime of oxide evaporation products in plasma.

Further, CeO_2 and CeO_2+Y_2O_3 films deposited via condensation of the evaporated material were analyzed. Polished silicon was used as a collector substrate. SEM images were obtained and EDX analysis of the formed coatings was performed.

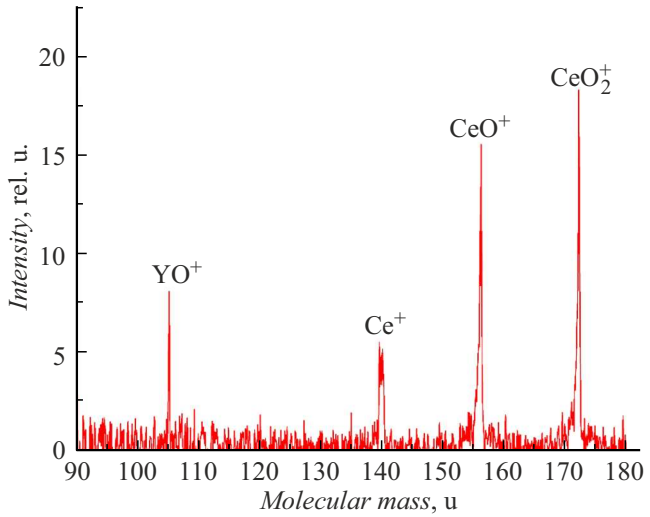

Figure 5. Mass spectrum reflecting the vapor composition during laser evaporation of the CeO_2 and Y_2O_3 mixture.

Typical SEM images of the material deposited in the upper collector are shown in Figure 6, *a*. The material consists of a cracked film.

Typical magnified image of the film end is shown in Figure 6, *b*. The film consists of filamentary crystallites predominantly with a dendritic structure, which is inherent in films, that are deposited at a high rate from gas phase on sufficiently cold surfaces [19,20]. Full identification of the uniform film deposition process modes with the single-phase laser blow-off mode in the presence plasma is known to be incorrect [21], therefore, a conclusion was made that the growth rate of this film corresponds to the weight loss rate of a target in the form of atoms and molecules and partially in the form of clusters thereof (for brevity the mean evaporation rate, Y). Separation efficiency is as high as possible when the plasma flow of separated substances contains only singly charged ions of light and heavy elements. If the flow has heavy charged molecular clusters of light elements, then their trajectory can slightly differ from that of heavy element ions, leading to overlapping of these flows and reduction of plasma separation efficiency.

Estimate of the proportion of molecular clusters in the vapor flow, investigations of cluster charging, behavior of their sizes and motion in the separator plasma to identify the degree of cluster impact on the plasma separation process characteristics can turn out to be an important part of further process development. Note here that according to the reported data, formation of a significant amount of clusters depends on the target material and is specific only for particular condition ranges. Thus, in [22], when semiconductor materials were exposed to 1064 nm nanosecond radiation pulses, clusters (up to 10 % of the total amount of particles) were observed in ablation products only in a limited power density range of $2-4 \cdot 10^8$ W/cm^2.

In [16], with laser time and power properties that are close to our properties, it was found that several complex substances change from the incongruent to cluster type of evaporation as the power density increases within 10^6-10^7 W/cm^2. However, this dependence is not typical of evaporation of targets studied in this work.

Table 1 shows the atom concentration ratios [Ce]:[Y] observed in deposited films after the first pass of the scanning segment with the specified laser power density. EDX analysis of the deposited film has shown predominant content of Ce with respect to Y in the evaporated material. This qualitatively corresponds to incongruent evaporation of materials with substantially different pressures of saturated vapors at a set temperature (sublimation heat of CeO_2 and reaction heat, at which sublimation of Y_2O_3 takes place: 562 kJ/mol and 2116 kJ/mol, respectively [23]). Thus, gas stripping of cerium from the mixture surface takes place at the initial laser evaporation stage. Considerable growth of [Ce]:[Y] in the film , as I_0 increases in a significant part of the range of interest (Table 1), is opposite to the trend, which, according to [16], serves as a sign of the cluster type of evaporation of complex substances during

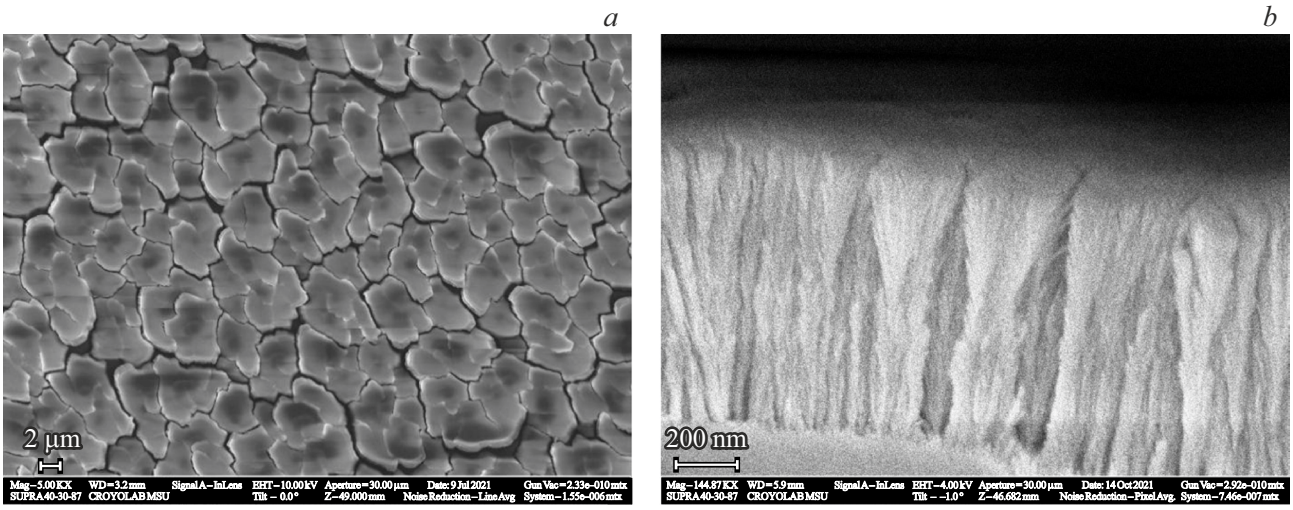

Figure 6. *a* — image of the surface of cerium oxide film deposited on a silicon substrate with a laser power of $2.3 \cdot 10^6$ W/cm^2; *b* — magnified image of the end of separated crystal film deposited via vapor condensation on the collector.

laser evaporation in this range of I_0. Therefore, it is suggested that the proportion of clusters in the vapor flow is insignificant during evaporation of the targets of interest in the given range of I_0 , therefore it shall not have any considerable effect on separation efficiency.

At a high power density, atomic ratio in the film after the initial pass reaches 20 (compared with the atomic ratio in the target 0.9, it has changed by a factor of 22). Accordingly, the rate of Y_2O_3 evaporation from mixture is very low (less than 1 g/h), and this can explain the reported absence of Y^+ in the vapor spectrum (Figure 5). Note that , when a solid solution based on the Y_2O_3 mixture with simulated UO_2 is evaporated from the effusion cell, significant differences in the volatility of individual oxides lead to predominant stripping of UO_2 from the solution [24].

Observed dependences can be explained qualitatively by the fact that during Y_2O_3 evaporation, unlike CeO_2, steady-state („developed“) evaporation time threshold is overcome only at intensities near the upper limit, on the order of $2.3 \cdot 10^6$ W/cm^2. Therefore, predominant evaporation of cerium oxide takes place in most of the I_0range.

The experiment has shown that during further evaporation this ratio and gas stripping efficiency decrease; behavior of [Ce]:[Y] in deposited films with each new pass of the surface by the beam at $I_0 = 1.1 \cdot 10^6$ W/cm^2 is shown in Figure 7. Pure silicon substrate was placed into the collector assembly before a pass with the corresponding number.

It can be seen that [Ce]:[Y] in the film (and therefore in vapor) decreases with each successive pass, and after pass 7–8 approaches the steady-state ratio, which is close to the element ratio in the initial target.

Figure 8 shows the mass evaporation rate measurements of a two-component target, each of which was obtained after expiration of the specified number of passes of the target by the laser beam at $I_0 = 1.1 \cdot 10^6$ W/cm^2 (at a mean laser power of 125 W).

From the experimental data shown in Figure 8, it follows that the mass evaporation rate of the two-component target decreases at the initial evaporation stages; it approached the evaporation rate of the simple yttrium oxide target (8 g/h and 6 g/h, respectively) after the fifth pass and doesn't decrease further. The initial decrease in the evaporation rate can be explained qualitatively by the fact that the evaporated target layer and, accordingly, the vapor composition are enriched with the least volatile yttrium oxide with each pass as mentioned above (Figures 4 and 7).

Since the initially high gas stripping efficiency decreases considerably as a result of following laser beam passes over the target surface (over the solidified melt), a cerium atom enrichment algorithm shall be built for this simulated mixture to ensure gas stripping. The algorithm shall include removal of the top of melt before the next evaporation

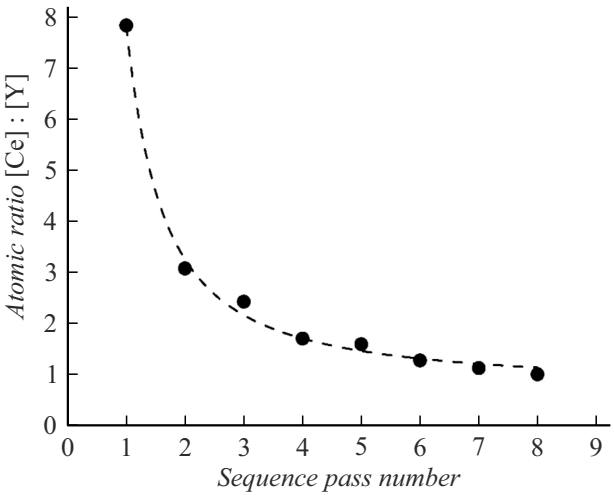

Figure 7. Behavior of [Ce]:[Y] in deposited films with each new pass.

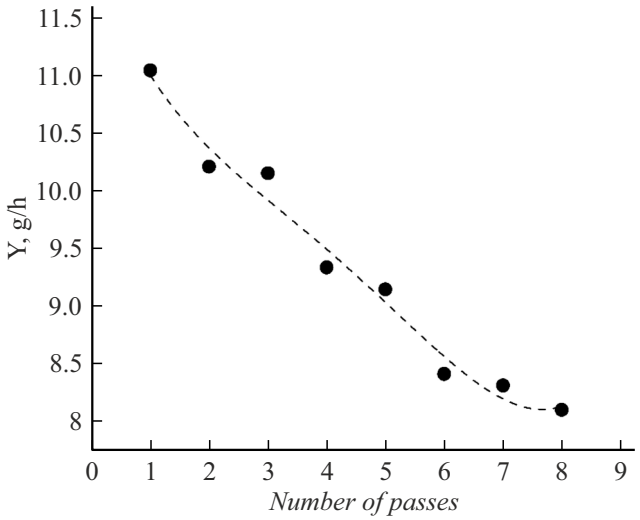

Figure 8. Mean mass evaporation rate measurements of a two-component target.

Figure 9. Target pressed without sintering after laser exposure. Full separation of the molten surface layer from the main target body is obvious.

iteration. Preliminary observations show that such removal is possible, when using two-component targets with the same composition, but having a lower apparent density. Experiments with targets pressed from micron-size powders without further sintering have detected that separation of the molten top layer of the sample was possible at moderate laser exposure powers, 20 %−40 % of the maximum power. Most of the target in this case is not destructed and is still structured. Figure 9 shows a photograph of a pressed target after exposure to laser radiation with a power density of $1.1 \cdot 10^6$ W/cm^2 and point exposure time of about 100 μs. Appearance of the sample suggests that separation of the top layer occurs after completion of laser exposure. Surface roughness after removal of the first „enriched layer“ is visually the same as that of the outer surface of the separated fragment. Separation occurs in one layer or a layer is fractured into two or three large parts after the first pass over a smooth surface. Therefore, with horizontal horizontal positioning of the evaporated surface, removal of this layer before the next pass is possible through a physical impact directly on the separated material. With vertical or inclined position of the evaporated surface, the molted layer can be removed, for example, by means of forced target vibration. Both methods will require provision of not too complex motion inputs into the separator chamber, for example, bellows type ones.

Small thickness of the separated material, dark inclusions into a newly formed target surface under the separated material together with depth distribution data for [Ce]:[Y] as shown in Figure 4 indicate that [Ce]:[Y] in the new surface (after removal of the separation) is on average a little lower than the initial ratio. The effect of this factor, target heating and change in the target relief with each iteration during long-term operation can depend on certain geometrical factors and target material properties, therefore it shall be studied separately.

2.3. Coarse fraction

Visual inspection of a coarse fraction collected on the lower collector has shown that evaporation of the CeO_2 and Y_2O_3 mixture is characterized by the presence of drops with an insignificant amount of target debris. As noted above in the introduction, the presence of a drop fraction for processes of conversion of the working medium into plasma necessitates the development of neutral component flow recirculation and filtration mechanisms. This is caused by the fact that conversion of drops, clusters and debris into plasma with a proportion of singly ionized atoms close to 1 is extremely difficult. This fact necessitates determination of a power density that provides the best ratio of the evaporation rate and material removal rate of the target in the form of drops, clusters and target debris.

Measurements have shown that a proportion of the coarse fraction in the CeO_2+Y_2O_3 target destruction products has no pronounced dependence on the evaporation time, at least, during the first 8 passes. Power density variation has shown that , during evaporation of the CeO_2+Y_2O_3 target, the mass coarse fraction L in destruction products increases when I_0 reaches $1.5 \cdot 10^6$ W/cm^2 in out experiments (Table 2); and the measured atomic ratio [Ce]:[Y] in drops turned out to be low (at a level of 0.15), close to the values inside the melt (Figure 4). Growth of L with significant cerium component depletion of drops corresponds to the observed sharp increase in [Ce]:[Y] in the film (and, thus, in the vapor phase) to 20 at a high power density of $1.9 \cdot 10^6$ W/cm^2 (Table 1).

Note that experiments didn't demonstrate cerium component enrichment of the surface of drops flying from the target, which is inherent in the top thin melt surface layer formed on the target after exposure (Figure 4). [Ce]:[Y] in drops is close to low values inside the melt because drops quickly leave the target surface immediately after formation

Table 1. [Ce]:[Y] in the deposited film as a result of ceramics evaporation in the first pass depending on the laser power density

Power density, W/cm^2	Initial sample	$3.0 \cdot 10^5$	$6.9 \cdot 10^5$	$1.1 \cdot 10^6$	$1.5 \cdot 10^6$	$1.9 \cdot 10^6$	$2.3 \cdot 10^6$
[Ce]:[Y] in film	0.9	8.7	6.1	8.8	9.1	20.0	18.4

Table 2. Dependence of the mass coarse fraction L on power density

Power density, W/cm^2	$3.0 \cdot 10^5$	$5.7 \cdot 10^5$	$6.9 \cdot 10^5$	$1.1 \cdot 10^6$	$1.5 \cdot 10^6$	$1.9 \cdot 10^6$	$2.3 \cdot 10^6$
L, %	3.1	3.9	5.5	6.0	15.5	21.7	26.1

and are not exposed to the vapor flow enriched with cerium components.

Since it is not possible to avoid the occurrence of drops in the vapor flow (with the existing evaporation efficiency requirements), consider separation of the vapor and drop flows from each other. Estimated film thickness (vapor condensate) distribution across the collector has shown that the main part of the evaporated material vapor flow propagates to the top of collector. This observation qualitatively corresponds to the data found earlier for the given power density range: during laser evaporation of a flat target, directional pattern maximum of the vapor flow is near the normal to the surface, and angular distribution of the vapor flow density is closer to cosine type [25]. By contrast, video surveillance of the scatter trajectories of incandescent coarse products of target destruction suggests that only a small amount of the products flies at large angles to the surface in our conditions. The melt flow on the initially flat target is known to obtain radial direction from the center of the laser spot along the surface when exposed to the vapor recoil momentum [25]. As the well grows, an axial melt flow component is added to the radial component due to the melt movement along the inclined wall; nevertheless, the resultant directional pattern of drop departure shall have its maximum by the angle to the surface, not coinciding with the normal direction; such picture during metal target evaporation was observed in [26,27]. For our future work, we are planning to provide conditions for reliable capture of escaping drops on substrates placed on the inner collector walls for further more detailed analysis of the directional pattern of drop scatter.

Conclusion

The study has demonstrated the possibility of steady-state evaporation of targets consisting of a refractory oxide mixture in conditions corresponding to plasma separation conditions (residual air pressure 0.04 Pa, distance to the target of about 1 m), at a rate of 10 g/h with low content of coarse fraction, by 1067 nm laser radiation with a mean radiation power of 125 W and power density of $1.1 \cdot 10^6$ W/cm^2. At the initial process stage, the highest evaporation rate of the oxide mixture reached 30 g/h at a power density of $2.3 \cdot 10^6$ W/cm^2 (mean power is 240 W). To meet the evaporation rate at a level of hundreds of grams per hour required of the vapor source for plasma separation, laser with higher mean power shall be used with the same or higher radiation power density; increase in the number of lasers in the evaporation unit can be one of the options. Evaporation of the CeO_2 and Y_2O_3 mixture is characterized by the presence of a drop fraction with a small amount of target debris. The proportion of coarse particles in the destruction products of a target containing a mixture of cerium and yttrium oxides grows from 6% to 25% by weight as I_0 increases from 1 to $2.3 \cdot 10^6$ W/cm^2. The study investigated the composition and structure of ceramic targets prepared from a mixture of CeO_2 and Y_2O_3 and used as a simulated vapor source for optimization of the SNF plasma separation process. For the development of a vapor source for a plasma separator, consider that evaporation in incongruent during several first target passes by the laser beam: surface layer of such targets acquires a new composition containing new crystal phases and having a significantly changed initial relative concentration of elements: melt layer is depleted with a more volatile component, cerium oxide in this case, which is stripped from the target before all others. These phenomena can be used to prepare the working medium for plasma separation. From a conceptual standpoint, this can make it possible to reduce the requirements for plasma separation process efficiency. Angular distribution maxima of the vapor flow density and drop scatter are spaced apart, which will provide a vapor flow with variables meeting the requirements for a plasma source for a plasma separator.

Acknowledgments

The authors would like to thank A.A.Tatarintsev, Candidate of Physical and Mathematical Sciences, Senior Research Associate, for conducting the EDX analysis of experimental samples.

Funding

The study was supported by the Ministry of Science and Higher Education of the Russian Federation (State Order No. 075-00269-25-00).

Conflict of interest

The authors declare no conflict of interest.

References

[1] G. Liziakin, N. Antonov, V.S. Smirnov, R. Timirkhanov, A. Oiler, R. Usmanov, A. Melnikov, N. Vorona, S. Kislenko, A. Gavrikov. J. Phys. D: Appl. Phys., **54** (41), 414005 (2021). https://doi.org/10.1088/1361-6463/ac128e
[2] B. Luther-Davies, V. Kolev, M. Lederer, N. Madsen, A. Rode, J. Giesekus, K. Du, M. Duering. Appl. Phys. A, **79** (4), 1051 (2004). https://doi.org/10.1007/s00339-004-2626-x
[3] E.G. Gamaly, A.V. Rode, B. Luther-Davies. J. Appl. Phys., **85** (8), 4213 (1999). https://doi.org/10.1063/1.370333
[4] Y.A. Kotov, V.V. Osipov, O.M. Samatov, M.G. Ivanov, V.V. Platonov, A.M. Murzakaev, E.I. Azarkevich, A.I. Medvedev, A.K. Shtolts, O.R. Timoshenkova. Tech. Phys., **49** (3), 352 (2004). https://doi.org/10.1134/1.1688424
[5] G. Staupendahl, G. Michel, G. Eberhardt, E. Müller, Ch. Oestreich, W. Vogelsberger, J. Schlegel. J. Laser Appl., **11** (1), 14 (1999). https://doi.org/10.2351/1.521874
[6] V.V. Osipov, V.V. Platonov, V.V. Lisenkov, E.V. Tikhonov, A.V. Podkin. Appl. Phys. A, **124** (3), 3 (2018). https://doi.org/10.1007/s00339-017-1348-9
[7] V.A. Petrov. High Temperature, **54** (2), 186 (2016). https://doi.org/10.1134/S0018151X16020140]
[8] R.A. Usmanov, R.Kh. Amirov, A.V. Gavrikov, G.D. Liziakin, A.D. Melnikov, V.P. Polistchook, I.S. Samoylov, V.P. Smirnov, N.A. Vorona, I.M. Yartsev. Plasma Sources Sci. Technol., **29** (1), 015004 (2020). https://doi.org/10.1088/1361-6595/ab5f33
[9] A.T. Nelson, D.R. Rittman, J.T. White, J.T. Dunwoody, M. Kato, K.J. McClellan. J. Am. Ceram. Soc., **97** (11), 3652 (2014). https://doi.org/10.1111/jace.13170
[10] W. Tropf, D. Harris. Window and Dome Technol. Mater., **1112**, 9 (1989). https://doi.org/10.1117/12.960758
[11] N.M. Aristova. High Temperature, **60** (6), 756 (2022). https://doi.org/10.1134/S0018151X22040095
[12] S.I. Anisimov, Ya.A. Imas, G.S. Romanov, Yu.V. Khodyko, *Deistvie izlucheniya bol'shoi moshchnosti na metally* (Nauka, M., 1970) (in Russian).
[13] N.I. Koroteev, L.I. Shumai. *Fizika moshchnogo lazernogo izlucheniya.* (Nauka, M., 1991), 309 s.(in Russian)
[14] Electronic source. ICDD databasePDF-2. International Centre for Diffraction Data, URL: https://www.icdd.com/pdf-2 (Date of access: 15.02.2025)
[15] J. Xu, R. Xi, X. Xu, Y. Zhang, X. Feng, X. Fang, X. Wang. J. Rare Earths, **38** (8), 840 (2020). https://doi.org/10.1016/j.jre.2020.01.002
[16] M.V. Gerasimov, Yu.P. Dikov, O.I. Yakovlev. Petrologiya, **20** (5), 439 (2012).(in Russian)
[17] V. Piacente, G. Bardi, L. Malaspina, A. Desideri. J. Chem. Phys., **59** (1), 31 (1973). https://doi.org/10.1063/1.1679807
[18] L.L. Ames, P.N. Walsh, D. White. J. Phys. Chem., **71** (8), 2707 (1967). https://doi.org/10.1021/j100867a049
[19] J.A. Thornton, J. Vac. Sci. Technol., **11** (4), 666 (1974). https://doi.org/10.1116/1.1312732
[20] V. Haas, R. Birringer. Nanostructured Mater., **1** (6), 491 (1992). https://doi.org/10.1016/0965-9773(92)90082-9
[21] A. Richter. Thin Solid Films, **188** (2), 275 (1990). https://doi.org/10.1016/0040-6090(90)90290-T
[22] A.V. Bulgakov, A.B. Evtushenko, Yu.G. Shukhov, I. Ozerov, V. Marin. Kvantovaya elektronika, **40** (11), 1021 (2010) (in Russian).
[23] E.K. Kazenas, D.M. Chizhikov. *Davlenie i sostav para nad okislami khimicheskikh elementov* (Nauka, M., 1976), 342 s. (in Russian)
[24] E.K. Kazenas. *Termodinamika ispareniya dvoinykh oksidov* (Nauka, M., 2004), 550 s. (in Russian)
[25] D.R. Olander. Pure Appl. Chem., **62** (1), 123 (1990). http://dx.doi.org/10.1351/pac199062010123
[26] V.K. Goncharov, K.V. Kozadaev, M.V. Puzyrev, D.L. Slavashevich. Inzhenerno-fizicheskii zhurn., **81** (2), 211 (2008). (in Russian) https://doi.org/10.1007/s10891-008-0027-2
[27] V.K. Goncharov, G.A. Gusakov, V.I. Popechits, M.V. Puzyrev. Vestnik BGU, **3**, 50 (2013).(in Russian)

Translated by E.Ilyinskaya